

Strong room-temperature ferromagnetism in VSe₂ monolayers on van der Waals substrates

Manuel Bonilla, Sadhu Kolekar, Yujing Ma, Horacio Coy Diaz, Vijaysankar Kalappattil, Raja Das, Tatiana Eggers, Humberto R. Gutierrez, Manh-Huong Phan and Matthias Batzill*

Reduced dimensionality and interlayer coupling in van der Waals materials gives rise to fundamentally different electronic¹, optical² and many-body quantum³⁻⁵ properties in monolayers compared with the bulk. This layer-dependence permits the discovery of novel material properties in the monolayer regime. Ferromagnetic order in two-dimensional materials is a coveted property that would allow fundamental studies of spin behaviour in low dimensions and enable new spintronics applications⁶⁻⁸. Recent studies have shown that for the bulk-ferromagnetic layered materials CrI₃ (ref. ⁹) and Cr₂Ge₂Te₆ (ref. ¹⁰), ferromagnetic order is maintained down to the ultrathin limit at low temperatures. Contrary to these observations, we report the emergence of strong ferromagnetic ordering for monolayer VSe₂, a material that is paramagnetic in the bulk^{11,12}. Importantly, the ferromagnetic ordering with a large magnetic moment persists to above room temperature, making VSe₂ an attractive material for van der Waals spintronics applications.

Layered van der Waals materials have shown strong variations of their properties as they are thinned to a single molecular layer. These include: (1) transitions from an indirect to a direct bandgap material^{1,2}, thus opening new opportunities for optoelectronic applications¹³; (2) variations of many-body quantum criticalities, such as charge density wave (CDW)^{3,4} or superconducting⁵ transitions; and (3) field tunability of many-body states^{10,14,15}. The variety of physical properties in two-dimensional (2D) materials together with the potential to arbitrarily combine materials with atomically sharp interfaces makes them promising for designing heteromaterials that exhibit novel properties or enabling new device architectures^{16,17}. Monolayer ferromagnetic materials would be an important addition to the family of 2D materials. Such materials have great potential for spintronics, that is, use of the spin degree of freedom of electrons rather than their charge, as such devices rely on nanomaterials with dimensions smaller than the spin relaxation length and controlled interface properties. This potential was realized soon after the isolation of graphene, the first true 2D material, and attempts have been made to induce magnetism by proximity to ferromagnetic materials, adsorption, defects or doping of 2D materials¹⁸⁻²⁰. However, such disordered systems have generally low magnetic moments and are not suitable for applications. Accordingly, layered materials with intrinsic magnetic ordering have been sought, mainly focusing on materials with ferromagnetic order in the bulk²¹⁻²⁴. Recent advances in thinning such bulk-ferromagnetic materials to a single⁹ or bilayer¹⁰ have demonstrated that ferromagnetic order can persist to this ultrathin limit, despite predictions by the Mermin-Wagner theorem²⁵ that long-range magnetic order should be suppressed at finite temperatures in 2D materials.

The most versatile family of 2D materials is the transition metal dichalcogenides (TMDs), which mainly exhibit two polymorphs, that is, the trigonal prismatic (2H) or octahedral (1T) structure. While TMDs with semiconducting, metallic, superconducting and CDW properties are known, no TMD exhibits intrinsic ferromagnetism in its bulk form. VSe₂ with a high spin V 3d (ref. ¹) state is paramagnetic^{11,12} in bulk form and commonly condenses in the 1T structure. Some controversy exists in density functional theory (DFT) prediction of the stable structure of monolayer VSe₂. Both of the 2H and 1T polymorphs have been invoked as the ground state and the correct answer may depend sensitively on taking the correlations of the V d-shell electrons into account by choosing a correct Hubbard U parameter in DFT + U simulations²⁶. While there is controversy regarding the structure, there is an agreement that the 2H phase would be semiconducting while the 1T phase remains metallic even in the monolayer form. DFT simulations also predict that the monolayer should exhibit ferromagnetic ordering with in-plane spin alignment for both the 1T and 2H phases²⁷⁻²⁹. Experimentally, the verification of magnetism in monolayer materials has been hampered by the chemical instability under ambient conditions, which has limited the study of exfoliation from bulk materials to a few layers³⁰. Here we succeed in synthesizing single- and few-layer VSe₂ by molecular beam epitaxy and enable ex situ magnetic characterization by protecting the film with a Se capping layer. The studies reveal a significant enhancement of the magnetic moment in single layers compared with multi-layer samples. Astonishingly, the ferromagnetic ordering is very robust and persists above room temperature, thus making VSe₂ a favourable material for van der Waals spintronics applications. Moreover, we show that a CDW transition, known for bulk VSe₂ (ref. ³¹) and few-layer samples³², is also observed for the single layer and that it couples with its magnetic properties.

VSe₂ was grown on graphite (highly oriented pyrolytic graphite (HOPG)) or MoS₂ by molecular beam epitaxy. The mono- to few-layer films were characterized by X-ray and ultraviolet photoemission spectroscopy (XPS and UPS) as well as scanning tunnelling microscopy (STM) in an analysis chamber attached to the growth chamber. After capping the films with an ~10 nm Se layer, the samples were characterized ex situ by various magnetic probes described below. As a control sample, a commercial 1T VSe₂ single crystal was cleaved in ultrahigh vacuum and also capped with Se to avoid spurious results from a surface oxidized sample. Figure 1 shows characterization of submonolayer VSe₂ films on HOPG and MoS₂ substrates. On HOPG, VSe₂ preferentially nucleates and grows at step edges while on MoS₂ the growth is more uniform and gives rise to larger monolayer islands. In general, films on MoS₂ gives better layer-by-layer growth while on HOPG the VSe₂ films roughen.

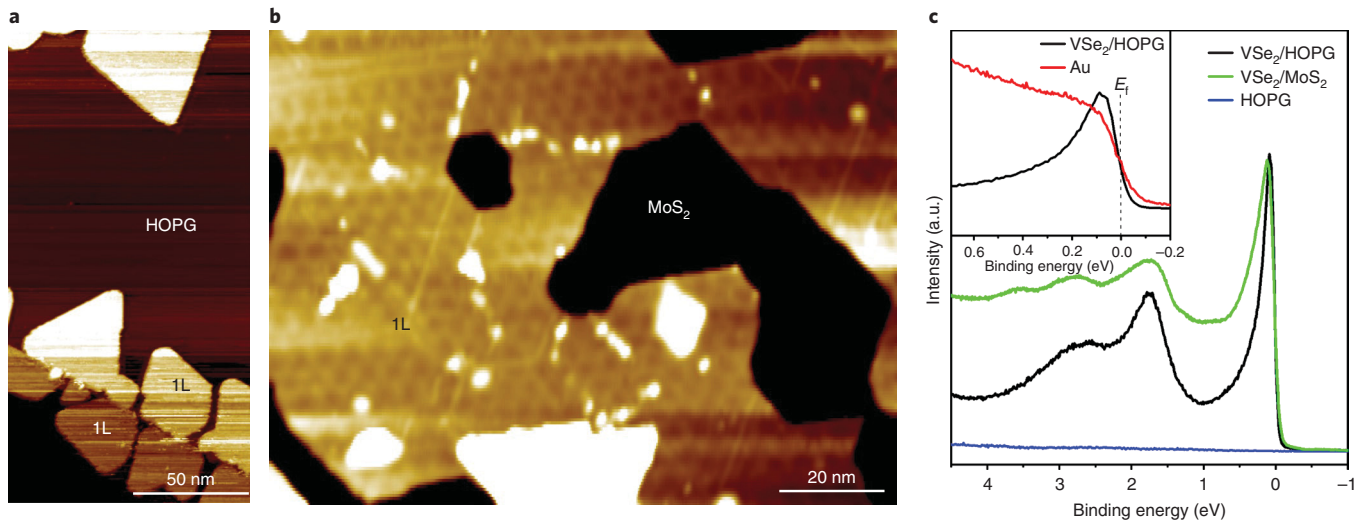


Fig. 1 | (Sub)monolayer VSe₂ films grown on HOPG or MoS₂ substrates characterized by STM and UPS. **a,b**, VSe₂ monolayer islands preferentially nucleate at step edges on HOPG (**a**), while they grow more uniform monolayer films on MoS₂ substrates (**b**). STM imaging parameters: bias voltage, $V_{\text{bias}} = 300$ mV; tunnelling current, $I_t = 0.9$ nA. A moiré structure for the VSe₂ monolayer (1L) on MoS₂ is observed due to the lattice mismatch between film and substrate. **c**, UPS measurements show a sharp metallic edge for both VSe₂ on HOPG and MoS₂ substrates consistent with the 1T structure of VSe₂. The inset shows a comparison of the Fermi edge (E_F) of VSe₂ films and a gold reference sample.

The monolayer VSe₂ on MoS₂ exhibits a moiré structure arising from the lattice mismatch between VSe₂ and MoS₂. XPS studies for estimation of the growth rates are shown in Supplementary Fig. 1. UPS shows a strong metallic edge, shown in Fig. 1c, which is consistent with a 1T metallic structure of VSe₂.

Importantly, to confirm a 1T metallic state, the samples were investigated for CDW transitions that can occur only in metallic samples. STM measurements at elevated (150 K) and low temperature (15 K), shown in Fig. 2a and 2b, respectively, revealed a CDW modulation at low temperature only. This demonstrates the existence of a CDW transition even for the monolayer VSe₂. It has been shown that the Fermi-surface nesting vector has a 3D component in

the bulk³¹ and thus the CDW in a strictly 2D single layer material will require a different nesting vector. This may explain the CDW periodicity observed in STM for the monolayer, which resembles the previously reported CDW for decoupled layers formed by intercalation of atoms³³, but is different from a 4×4 structure observed on bulk surfaces. Scanning tunnelling spectroscopy (STS) at 15 K also showed opening of an ~ 55 meV gap (Fig. 2c) compared with STS at 150 K, a temperature above the CDW transition.

The Se-capped VSe₂ films were rapidly transferred to a physical property measurement system or longitudinal magneto-optic Kerr effect (L-MOKE) magnetometer. XPS analysis indicates that such protected VSe₂ films are stable in air for days (see Supplementary Fig. 2). All magnetization measurements were done within the same day of exposure to air.

First, we discuss the magnetization measurements for VSe₂ films on HOPG. For a sample that consists of only monolayer height VSe₂ islands with coverage of approximately half a monolayer, the well-defined magnetization–magnetic field (M – H) hysteresis loops, observed at 10 and 330 K with vibrating sample magnetometry (VSM; Fig. 3a), show clear evidence for ferromagnetic ordering. The room-temperature ferromagnetism is also independently probed by L-MOKE (see inset of Fig. 3a). Control experiments on a HOPG substrate with a Se capping layer but without a VSe₂ film only show a diamagnetic background (see Supplementary Fig. 3). Consequently, the ferromagnetic signal is assigned to the single layer of VSe₂. This is an important finding considering that bulk VSe₂ is paramagnetic (see Supplementary Fig. 4). We also confirmed that the surface of VSe₂ has no ferromagnetic ordering by cleaving a VSe₂ single crystal in UHV and capping it with Se (also shown in Supplementary Fig. 4). Comparative in-plane and out-of-plane M – H loop VSM measurements of the monolayer sample are shown in Fig. 3b and indicate in-plane spin alignment, which is consistent with DFT predictions for monolayer magnetism of VSe₂ (refs 26–28). The temperature dependences of the coercive field (H_c) and saturation magnetization (M_s) up to 330 K (Fig. 3c) verify strong ferromagnetic ordering above room temperature for monolayer VSe₂/HOPG. Both the temperature dependence of H_c and M_s as well as the large value of M_s , which is estimated to be $\sim 15 \mu_B$ per formula unit, suggest that the magnetization is intrinsic to the VSe₂ monolayer/HOPG sample. DFT calculations have suggested through-bond spin

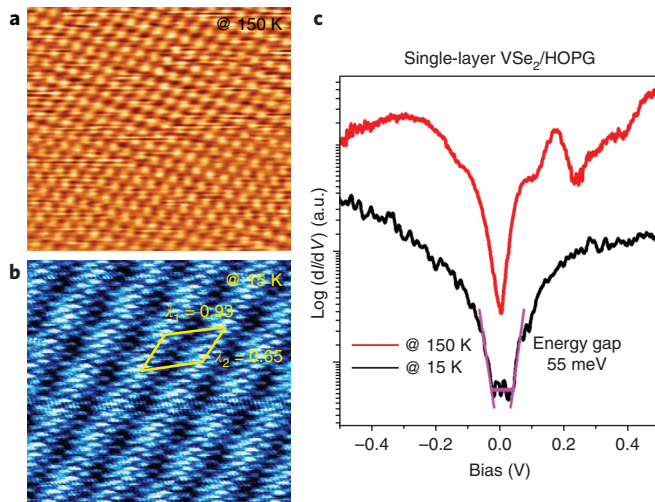


Fig. 2 | Evidence for CDW transition in monolayer VSe₂. **a,b**, STM images showing atomic corrugation above the CDW transition (150 K) (**a**) and CDW modulation of atomic corrugation below T_{CDW} (**b**). In **b** the CDW unit cell is indicated in yellow together with the approximate periodicities λ_1 and λ_2 , consistent with previously reported values in ref. ³³. STM imaging parameters: $V_{\text{bias}} = 700$ mV and $I_t = 0.6$ nA. **c**, STS shows the opening of an energy gap at low temperatures, which is extracted by the tangential approximation of the differential conductance shown by the pink lines in **c**.

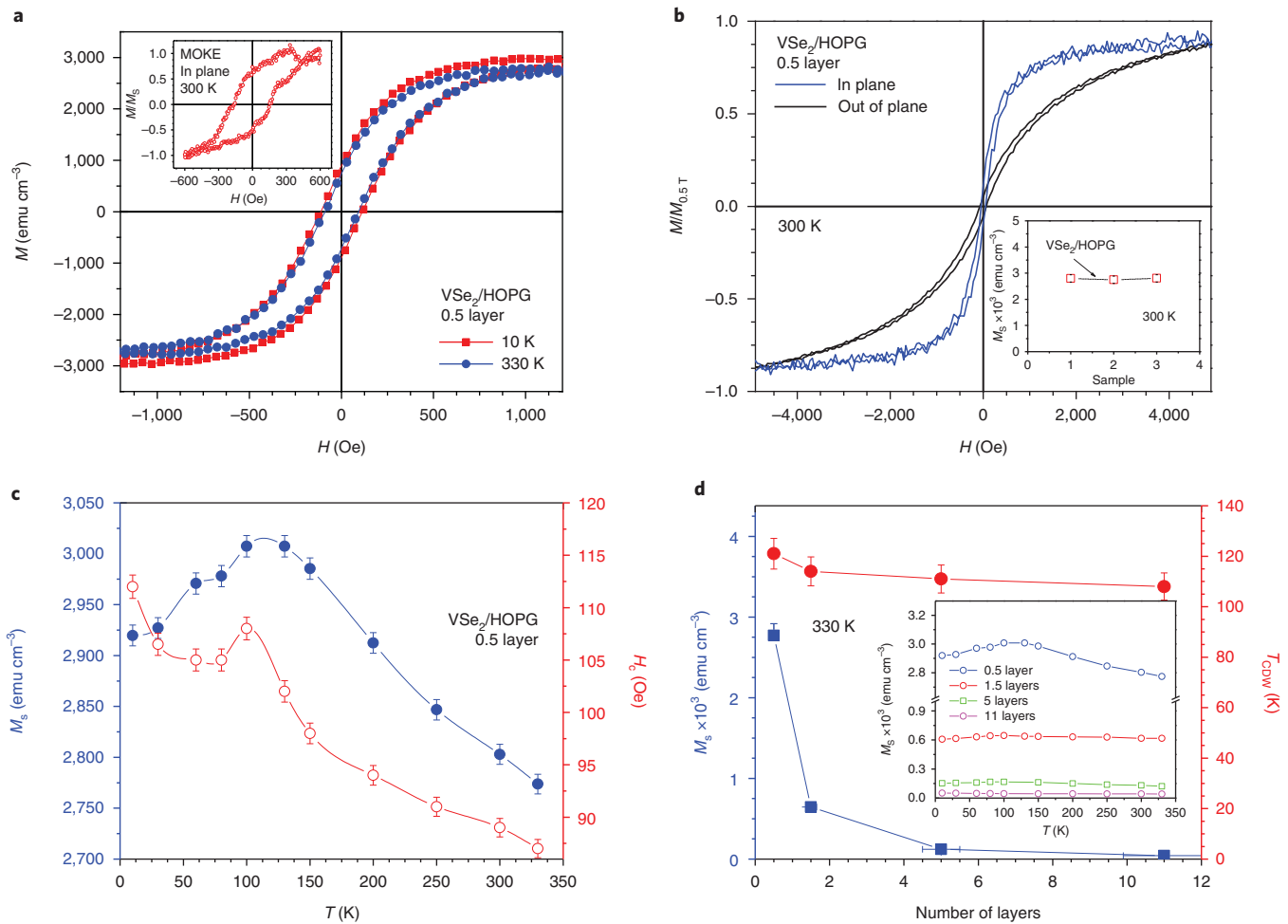


Fig. 3 | Magnetic properties of VSe₂ films on HOPG substrates. **a**, M - H hysteresis loops taken at 10 and 330 K. The inset shows the in-plane L-MOKE loop at 300 K. **b**, The in-plane and out-of-plane M - H loops at 300 K for monolayer VSe₂ on HOPG. The inset shows the reproducible values of M_s at 300 K for different VSe₂ monolayer samples grown on HOPG. **c**, Temperature dependences of H_c and M_s for monolayer VSe₂ islands. The variation in M_s and H_c around 120 K is indicative of the coupling of magnetism to the CDW that is enhanced in the monolayer. **d**, Variations in M_s and variation of the non-monotonous behaviour associated with T_{CDW} with the number of layers of VSe₂ film. The inset shows the temperature dependence of M_s for all samples studied. The error bars for H_c , M_s and T_{CDW} are standard deviations obtained by repeating the measurements three times for the same sample. In **d**, uncertainties in the layer thickness derived from XPS (see Supplementary Fig. 1) and STM surface roughness are also indicated.

polarization between V and Se to be the origin for intrinsic ferromagnetic ordering in monolayer VSe₂ (ref. ²⁷). Such a mechanism may also explain the observed large magnetic moment in the samples presented here. The temperature dependence of M_s indicates the persistence of ferromagnetic order above room temperature for all monolayer VSe₂ samples studied, which show very reproducible values for magnetic properties of the film (see inset of Fig. 3b). It is interesting to point out that the monolayer VSe₂ sample exhibits a non-monotonic behaviour in M_s and H_c in a range around 110–130 K. This non-monotonic behaviour is ascribed to the CDW transition observed in STM and is expected in this temperature range³². Coupling of the magnetic properties to the CDW in VSe₂ further confirms that the observed magnetism is a property of VSe₂. A noticeable shift in the CDW transition temperature (T_{CDW}) to a higher temperature for the monolayer ($T_{CDW} \sim 121$ K) relative to bi- (~114 K) and multi- (~108 K) layers is consistent with recent reports on the thickness-dependence of the T_{CDW} in exfoliated VSe₂ flakes³². The T_{CDW} is also independently determined from the slope change in magnetization under zero-field-cooled and field-cooled regimes (see Supplementary Fig. 5). Increasing the number of layers is found to drastically decrease M_s (see inset of Fig. 3d).

To further study the magnetic properties of single-layer VSe₂ and to exclude a special influence of the HOPG substrate on the magnetic properties, we also investigated VSe₂ grown on MoS₂. The previously reported weak defect-induced ferromagnetism in MoS₂ single crystals³⁴ is confirmed (Supplementary Fig. 4c), but is much weaker than the magnetism of monolayer VSe₂ and thus cannot explain the magnetization measured in monolayer VSe₂. Figure 4a shows the VSM measurement of a mostly monolayer VSe₂ sample at room temperature and at 100 K. It is apparent that the temperature dependence for VSe₂ on MoS₂ is strongly enhanced compared with HOPG substrate, which is also illustrated in Fig. 4b. Such difference in the temperature dependence suggests enhanced magnetic coupling between the MoS₂ substrate and the ferromagnetic VSe₂ film. Importantly, like on HOPG, a strong variation of H_c is observed close to the expected CDW temperature. Figure 4c and its inset show measurements of the magnetic properties as a function of film thickness. Similar to the VSe₂ films on HOPG, a strong enhancement of M_s is observed when the film thickness is reduced to a single monolayer. Interestingly, only the monolayer sample exhibits very strong temperature dependence of M_s and H_c , further supporting the special magnetic properties of the monolayer and indicating strong magnetic interlayer coupling

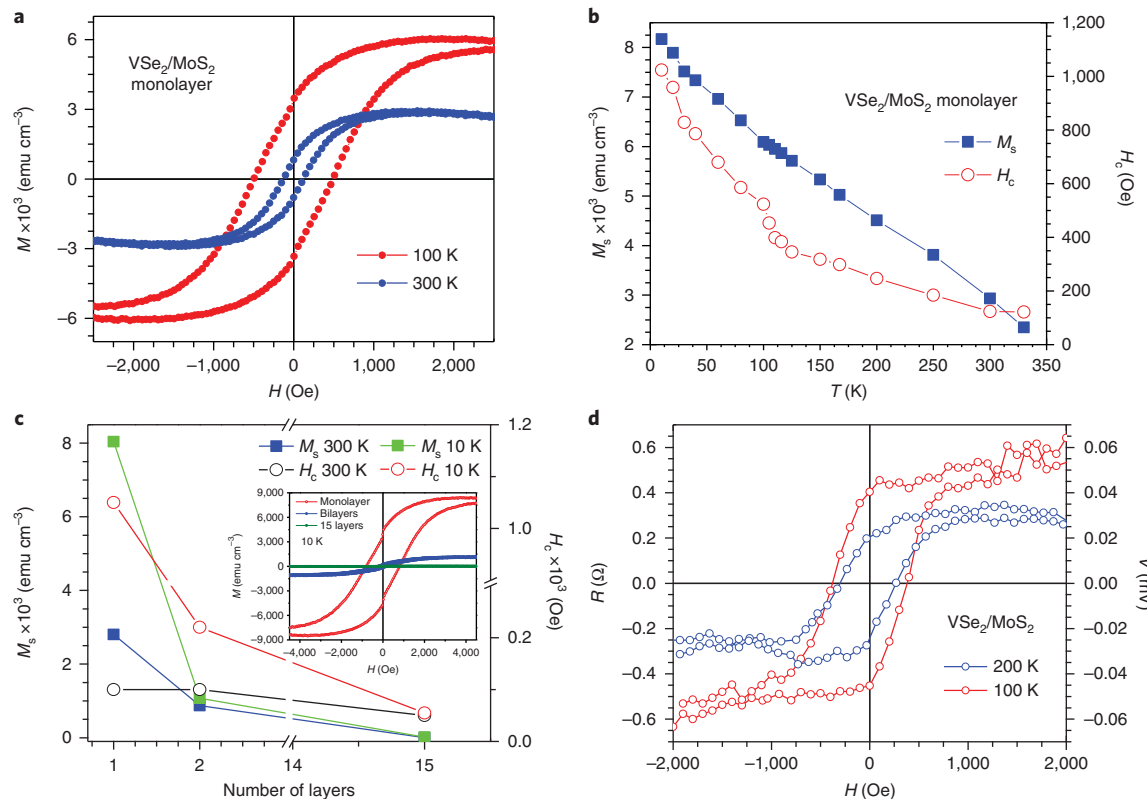


Fig. 4 | Magnetic properties of VSe₂ films on MoS₂ substrates. **a**, M-H loops taken at 100 K and 300 K for monolayer VSe₂. **b**, The strong temperature dependences of H_c and M_s . **c**, Variations of M_s and H_c with the number of layers of VSe₂ film. The inset shows the M-H loops for the mono-, bi- and multilayer samples. **d**, Anomalous Hall-effect measurements. Magnetic field dependences of resistance (R) and voltage (V) taken at 100 K and 200 K show clear hysteresis with larger loops at lower temperature (100 K versus 200 K), consistent with the temperature dependence of M-H loops observed by VSM.

between VSe₂ and MoS₂. Such interlayer couplings in magnetic van der Waals heterostructures illustrates the exciting prospects of these systems, which require further experimental and theoretical studies. Although the magnetization is drastically reduced with number of layers (Fig. 4c or 3d), it remains measurable to the thickest samples, tens of layers thick. This residual magnetization may be related to defects in the grown films or an interface polarization or Stark effect³⁵ that induces weak ferromagnetism in VSe₂ interfaces with dissimilar van der Waals materials. Finally, using a poorly conducting semiconducting van der Waals substrate, such as MoS₂, enables Hall measurements and thus an independent verification that the magnetism originates from the VSe₂ films. Using a shadow mask for VSe₂ deposition, we fabricated a Hall bar. The sample was mono- to bilayer thick to ensure a contiguous film. Figure 4d shows the hysteresis loops in this anomalous Hall-effect measurement at 100 K and 200 K, reproducing the temperature dependence of M_s and H_c measured by VSM. Thus the magnetization of monolayer VSe₂ on van der Waals substrates can be consistently probed by various complementary magnetic probes.

In conclusion, we have demonstrated ferromagnetism with a large magnetic moment in monolayer VSe₂/van der Waals heterostructures. A Curie temperature above room temperature makes these systems potentially attractive materials for van der Waals spintronics applications. Finally, the approach of molecular beam epitaxy growth and encapsulation provides an alternative to exfoliation methods for screening of theoretically predicted²⁹ monolayer TMDs, even if chemically unstable.

Methods

Methods, including statements of data availability and any associated accession codes and references, are available at <https://doi.org/10.1038/s41565-018-0063-9>.

Received: 28 May 2017; Accepted: 4 January 2018;
Published online: 19 February 2018

References

1. Mak, K. F., Lee, C., Hone, J., Shan, J. & Heinz, T. F. Atomically thin MoS₂: a new direct-gap semiconductor. *Phys. Rev. Lett.* **105**, 136805 (2010).
2. Splendiani, A. et al. Emerging photoluminescence in monolayer MoS₂. *Nano Lett.* **10**, 1271–1275 (2010).
3. Xi, X. et al. Strongly enhanced charge-density-wave order in monolayer NbSe₂. *Nat. Nanotech.* **10**, 765–770 (2015).
4. Kolekar, S., Bonilla, M., Ma, Y., Coy Diaz, H. & Batzill, M. Tunability of charge density wave criticality and evidence of an excitonic condensate in 1T-TiSe₂ monolayers. *2D Mater.* **5**, 015006 (2017).
5. Tsien, A. W. et al. Nature of the quantum metal in a two-dimensional crystalline superconductor. *Nat. Phys.* **12**, 208–212 (2016).
6. McCreary, K. M., Swartz, A. G., Han, W., Fabian, J. & Kawakami, R. K. Magnetic moment formation in graphene detected by scattering of pure spin currents. *Phys. Rev. Lett.* **109**, 186604 (2012).
7. Soumyanarayanan, A., Reyren, N., Fert, A. & Panagopoulos, C. Emergent phenomena induced by spin-orbit coupling at surfaces and interfaces. *Nature* **539**, 509–517 (2016).
8. Tong, W.-Y., Gong, S.-J., Wan, X. & Duan, C.-G. Concepts of ferrovalley material and anomalous valley Hall effect. *Nat. Commun.* **7**, 13612 (2016).
9. Huang, B. et al. Layer-dependent ferromagnetism in a van der Waals crystal down to the monolayer limit. *Nature* **546**, 270–273 (2017).
10. Gong, C. et al. Discovery of intrinsic ferromagnetism in two-dimensional van der Waals crystals. *Nature* **546**, 265–269 (2017).
11. van Bruggen, C. F. & Haas, C. Magnetic susceptibility and electrical properties of VSe₂ single crystals. *Solid State Commun.* **20**, 251–254 (1976).
12. Bayard, M. & Sienko, M. J. Anomalous electric and magnetic properties of vanadium diselenide. *J. Solid State Chem.* **19**, 325–329 (1976).
13. Xia, F., Wang, H., Xiao, D., Dubey, M. & Ramasubramaniam, A. Two-dimensional material nanophotonics. *Nat. Photon.* **8**, 899–907 (2014).
14. Yu, Y. et al. Gate-tunable phase transitions in thin flakes of 1T-TaS₂. *Nat. Nanotech.* **10**, 270–276 (2015).

15. Li, L. J. et al. Controlling many-body states by the electric-field effect in a two-dimensional material. *Nature* **529**, 185–189 (2016).
16. Geim, A. K. & Grigorieva, I. V. Van der Waals heterostructures. *Nature* **499**, 419–425 (2013).
17. Novoselov, K. S., Mishchenko, A., Carvalho, A. & Castro Neto, A. H. 2D materials and van der Waals heterostructures. *Science* **353**, aac9439 (2016).
18. Gonzalez-Herrero, H. et al. Atomic-scale control of graphene magnetism by using hydrogen atoms. *Science* **352**, 437–441 (2016).
19. Nair, R. R. et al. Spin-half paramagnetism in graphene induced by point defects. *Nat. Phys.* **8**, 199–202 (2012).
20. Avsar, A. et al. Spin–orbit proximity effect in graphene. *Nat. Commun.* **5**, 4875 (2014).
21. Li, X. & Yang, J. Cr₃Te₃ (X = Si, Ge) nanosheets: two dimensional intrinsic ferromagnetic semiconductors. *J. Mater. Chem. C* **2**, 7071–7076 (2014).
22. Zhang, W.-B., Qu, Q., Zhu, P. & Lam, C. H. Robust intrinsic ferromagnetism and half semiconductivity in stable two-dimensional single-layer chromium trihalides. *Mater. Chem. C* **3**, 12457–12468 (2015).
23. Lin, M.-W. et al. Ultrathin nanosheets of CrSiTe₃: a semiconducting two-dimensional ferromagnetic material. *J. Mater. Chem. C* **4**, 315–322 (2016).
24. Sun, Y., Zhou, Z., Wu, X. & Yang, J. Room-temperature ferromagnetism in two-dimensional Fe₃Si nanosheets with enhanced spin-polarization ratio. *Nano Lett.* **17**, 2771–2777 (2017).
25. Mermin, N. D. & Wagner, H. Absence of ferromagnetism or antiferromagnetism in one- or two-dimensional isotropic Heisenberg models. *Phys. Rev. Lett.* **17**, 1133–1136 (1966).
26. Popov, Z. I. et al. The electronic structure and spin states of 2D graphene/VX₂ (X = S, Se) heterostructures. *Phys. Chem. Chem. Phys.* **18**, 33047–33052 (2016).
27. Ma, Y. et al. Evidence of the existence of magnetism in pristine VX₂ monolayers (X = S, Se) and their strain-induced tunable magnetic properties. *ACS Nano* **6**, 1695–1701 (2012).
28. Fuh, H. R., Yan, B., Wu, S.-C., Felser, C. & Chang, C.-R. Metal–insulator transition and the anomalous Hall effect in the layered magnetic materials VS₂ and VSe₂. *New J. Phys.* **18**, 113038 (2016).
29. Lebègue, S., Björkman, T., Klintenberg, M., Nieminen, R. M. & Eriksson, O. Two-dimensional materials form data filtering and ab initio calculations. *Phys. Rev. X* **3**, 031002 (2013).
30. Xu, K. et al. Ultrathin nanosheets of vanadium diselenide: a metallic two-dimensional material with ferromagnetic charge-density-wave behavior. *Angew. Chem. Int. Ed.* **52**, 10477–10481 (2013).
31. Strocov, V. N. et al. Three-dimensional electron realm in VSe₂ by soft-X-ray photoelectron spectroscopy: origin of charge-density waves. *Phys. Rev. Lett.* **109**, 086401 (2012).
32. Pasztor, A., Scarfato, A., Barreteau, C., Giannini, E. & Renner, C. Dimensional crossover of the charge density wave transition in thin exfoliated VSe₂. *2D Mater.* **4**, 041005 (2017).
33. Ekwall, I., Brauer, H. E., Wahlström, E. & Olin, H. Locally modified charge-density waves in Na intercalated VSe₂ studied by scanning tunneling microscopy and spectroscopy. *Phys. Rev. B* **59**, 7751–7761 (1999).
34. Tongay, S., Varnoosfaderani, S. S., Appleton, B. R., Wu, J. Q. & Hebard, A. F. Magnetic properties of MoS₂: existence of ferromagnetism. *Appl. Phys. Lett.* **101**, 123105 (2012).
35. Zhang, Z. et al. Magnetic quantum phase transition in Cr-doped Bi₂(Se_xTe_{1-x})₃ driven by the Stark effect. *Nat. Nanotech.* **12**, 953–957 (2017).

Acknowledgements

This project was primarily supported by the National Science Foundation under grant DMR-1701390. V.K., R.D. and M.-H.P. also acknowledge support from the US Department of Energy, Office of Basic Energy Sciences, Division of Materials Sciences and Engineering under Award No. DE-FG02-07ER46438 and thank H. Srikanth for useful discussions.

Author contributions

M.Bo., S.K., H.C.D. and Y.M. synthesized samples and characterized and analysed the samples by STM, XPS and UPS. V.K. and R.D. performed magnetic characterization. T.E. carried out the L-MOKE experiments. H.R.G. performed Raman characterization. M.-H.P. and M.Ba. directed the research and wrote the manuscript. All authors contributed to the discussion of the data and commented on the manuscript.

Competing interests

The authors declare no competing financial interests.

Additional information

Supplementary information accompanies this paper at <https://doi.org/10.1038/s41565-018-0063-9>.

Reprints and permissions information is available at www.nature.com/reprints.

Correspondence and requests for materials should be addressed to M.B.

Publisher's note: Springer Nature remains neutral with regard to jurisdictional claims in published maps and institutional affiliations.

Methods

Molecular beam epitaxy growth. Mono- to few-layer VSe₂ was grown on HOPG or MoS₂ substrates by e-beam evaporation of V and simultaneous deposition of atomic Se from a hot wall Se-cracker source. The HOPG substrates were cleaved in air and immediately introduced into the vacuum chamber. The substrates were subsequently annealed in ultra-high vacuum at 300°C for 5 h before film growth. VSe₂ was grown at a substrate temperature of 300°C and at a slow growth rate of ~0.06 nm min⁻¹. After characterization of the grown films by UPS and STM, the samples were transferred back into the molecular beam epitaxy growth chamber and capped with ~10 nm of Se by deposition of Se at room temperature.

Photoemission characterization. For XPS and UPS measurements, the samples were transferred from the growth chamber with a magnetically coupled transfer arm to a surface analysis chamber without breaking vacuum. The mu-metal analysis chamber was equipped with an Omicron Sphera-II electrostatic analyser for UPS. For XPS, an Mg/Al dual anode X-ray source was used and for UPS, a vacuum ultraviolet He-discharge lamp was used. All measurements were acquired at normal emission. Mean free path lengths for photoelectrons were estimated based on the National Institute of Standards and Technology standards database. As a consequence of the varying mean free path lengths for V 3d and Se 2p photoelectrons, the probing depths of the two components varies and therefore the peak ratio changes for thinner films. After compensating for the different mean free path lengths, XPS shows the growth of stoichiometric VSe₂ films for all film thicknesses studied. For UPS measurements, the Fermi edge was calibrated with a gold sample.

Scanning tunnelling microscopy and spectroscopy. An Omicron room temperature STM-1 was also housed in the same surface characterization chamber used for UPS characterization. Electrochemically etched tungsten tips were used

for all the room temperature STM measurements. In addition, the sample was transferred in a vacuum suitcase that maintained a pressure of ~10⁻⁸ torr to a variable temperature STM. This STM is a commercial Pan-style RHK STM. A closed-cycle cryostat allowed cooling of the sample to a minimum of 15 K and the sample could be heated in the cryostat to various target temperatures. STM and STS was taken with a cut PtIr tip. For dI/dV spectroscopy, a lock-in amplifier with a modulation voltage of 7 mV and reference frequency of 995 Hz was used.

Physical property measurement system. Temperature- and magnetic field-dependent magnetization measurements were carried out in a physical property measurement system from Quantum Design with a vibrating sample magnetometer over a temperature range of 5–350 K and fields up to 7 T. Magnetic moment per formula unit for the monolayer was determined from the magnetization measurement (converted to Bohr magnetons) and divided by the number of formula units calculated from the sample size times the percentage of surface covered by a single layer and divided by unit cell size of VSe₂.

Magneto-optic Kerr effect. L-MOKE hysteresis loops were taken at room temperature using a homemade set-up with a 5 mW (655 nm) laser source with a spot size of ~1.5 × 1.5 mm².

Anomalous Hall effect. VSe₂ was deposited on a MoS₂ substrate through a shadow mask creating a Hall bar with four contacts. The grown VSe₂ film was subsequently capped with Se. After removal from the growth chamber, wires were glued with silver conducting paste onto the contact patches. The anomalous Hall measurements were performed in the physical property measurement system.

Data availability. The data that support the findings of this study are available from the corresponding author upon reasonable request.